


Consistent approach for electrical resistivity within Ziman's theory from solid state to hot dense plasma: Application to aluminum

Nadine Wetta¹* and Jean-Christophe Pain¹
CEA, DAM, DIF, F-91297 Arpajon, France

 (Received 24 August 2020; accepted 2 October 2020; published 16 November 2020)

The approach presented in this work allows a consistent calculation of electrical conductivity of dense matter from the solid state to the hot plasma using the same procedure, consisting in dropping elastic scattering contributions to solid's and liquid's structure factors in the framework of the Ziman theory. The solid's structure factor was computed using a multiphonon expansion. The elastic part is the zero-phonon term and corresponds to Bragg peaks, thermally damped by Debye-Waller attenuation factors. For the liquid, a similar elastic contribution to the structure factor results from a long-range order persisting during the characteristic electron-ion scattering time. All the quantities required for the calculation of the resistivities are obtained from our average-atom model, including the total hypernetted-chain structure factor used from the liquid state to the plasma. No interpolation between two limiting structure factors is required. We derive the correction to apply to the resistivity in order to account for the transient long-range order in the liquid and show that it improves considerably the agreement with quantum-molecular dynamics simulations and experimental aluminum's isochoric and isobaric conductivities. Our results suggest that the long-range order in liquid aluminum could be a slightly compressed fcc one. Two series of ultrafast experiments performed on aluminum were also considered, the first one by Milchberg *et al.* using short laser pulses and the second one by Sperling *et al.* involving x-ray heating and carried out on the Linac Coherent Light Source facility. Our attempts to explain the latter assuming an initial liquid state at an ion temperature much smaller than the electron one suggest that the actual initial state before main heating is neither perfectly solid nor a normal liquid.

DOI: [10.1103/PhysRevE.102.053209](https://doi.org/10.1103/PhysRevE.102.053209)

I. INTRODUCTION

The study of atomic properties of warm dense matter is of great interest in many fields of physics and drives a recurrent need for accurate equations of state as well as relevant transport coefficients. Among the latter, the electrical resistivity (and its inverse the conductivity) is of particular importance in simulations to model the intense energy-flux interactions with matter, like those encountered in laser-fusion experiments [1,2] or the study of planetary interiors [3].

Aluminum is one of the most studied materials under various conditions of densities and temperatures, in relation to both experimental techniques and theoretical methods. Aluminum's transport properties, and in particular static ones, have been the subject of many experimental approaches, among which techniques using high intensity heavy-ion beams [4] to probe large volumes of high-energy matter, pulsed electrical currents to explode wires [5,6] or to rapidly heat aluminum foils [7,8], z-pinch [9], isochoric heating in the "isochoric plasma closed vessel" facility [10,11], highly bright x-ray beams [12], or intense laser beams [13] to isochorically heat solid targets. Most of these studies investigate electrical transport properties of hot expanded aluminum in the liquid and plasma states. Besides these works, a great amount of data and information on solid aluminum's electrical

resistivity has been compiled and analyzed by Desai *et al.* [14]. The recent experiments performed by Brandt and Neuer confirm the reliability of these data [15]. Adding those of Milchberg *et al.*, they provide a set of experimental resistivities at densities close to aluminum's normal one (i.e., $\rho_0 = 2.7 \text{ g/cm}^3$) covering four orders of magnitude over ambient temperature. Additional data relative to liquid aluminum up to 4000 K from isobaric expansion experiments published by Gathers [16] can complete this set in the liquid area at the condition to keep in mind that they correspond to isobaric densities, somewhat lower than the normal one.

In the past few decades, considerable progress has been made in developing theoretical methods to explain available experimental data and predict behavior in conditions out of reach by experimental means. *Ab initio* quantum-molecular-dynamics (QMD) calculations [17–21] are believed to provide the most accurate results but are time-consuming and for this reason practicable only within a limited temperature range, typically about tens of eV. Therefore, extended calculations of transport properties are based on less expensive methods like the chemical-picture [22–24], coupled with the Zubarev method [25] and average-atom (AA) models [26–28] using approximations such as the relaxation-time one [29], the extended Ziman formula [30,31], or the Kubo-Greenwood (KB) approach [32,33]. Some comparisons between AA methods and QMD ones are presented in Refs. [34,35]. Average-atom models associated to the Ziman approach are used for instance in Refs. [28,36–38] to investigate aluminum's electrical

*nadine.wetta@cea.fr

resistivities, while Ref. [34] reports studies combining the average-atom model to the Kubo-Greenwood approximation.

One of the most important issues for relevant electrical resistivities with Ziman theory is to provide appropriate temperature and density-dependent ion-ion structure factors $S(k)$, the quantity $[S(k) - 1]$ being the Fourier transform of the ion pair correlation function $g(r)$, which gives the probability of finding an ion at the radius r . A number of theoretical works attempt to include descriptions of the ionic fluid and of the ion-ion potential in AA models with various degrees of self-consistency [39,40]. Others look instead for approximations to the structure factor, relying on the assertion that the detailed description of the structure factor is not of critical importance on resistivities, since electron Fermi-Dirac statistics selects a limited range of momentum around the Fermi one.

Calculation of the liquid's resistivity in the framework of Ziman's theory involves the ion structure factor in its wholeness, whereas, for the solid, it is replaced by an effective one, where the contribution of Bragg scattering (i.e., coherent or elastic scattering) is dropped from the total structure factor,

$$S_{\text{eff}}(\vec{k}) = S(\vec{k}) - e^{-2W(k)}S_0(\vec{k}), \quad (1)$$

as prescribed by Rosenfeld and Stott [41]. $S_0(\vec{k})$ is the structure factor for the perfect rigid lattice and $e^{-2W(k)}$ the Debye-Waller factor accounting for thermal damping. Elastic contributions have to be subtracted from the total structure factor for solid's resistivity calculation since the rigid periodic ion configuration does not disturb electron propagation and therefore does not induce electrical resistivity. Only the thermal fluctuations around the positions of the ions in this static configuration contribute to the latter. Baiko *et al.* [42,43] affirm that long-range order persists in the liquid during typical electron-ion scattering time, justifying the extension of Rosenfeld and Stott's prescription to liquids. Baiko *et al.*'s assumption has been applied by Ovechkin *et al.* [44] to liquid aluminum at normal density and temperature $T \gtrsim 0.1$ eV within INFERNO [45] and the neutral ion-sphere-based AA methods [46]. Despite the fact that they used a crude approximation for the inelastic structure factor (i.e., the remaining part of the structure factor once the elastic contributions are subtracted), the authors observed overall better match with available QMD results than when total structure factors are used. Hansen *et al.* [47] came to the same conclusion.

In the present paper, we consider the issue of removing the elastic contribution to the ion-ion structure factor for electrical resistivity calculation in warm-dense matter. We focus our attention on the case of normal density aluminum's electrical resistivity, for which a great number of experimental [13–16] and theoretical [17–20] results are available from ambient temperature up to 100 eV. For the solid state, $S(k)$ is written as a multiphonon expansion and the necessary number of terms to obtain converged inelastic $S_{\text{inel}}(k)$ for face-centered cubic (fcc) aluminum is computed. The latter structure factor is then identified with the effective one to be used, as prescribed by Rosenfeld *et al.*, for the calculation of solid's resistivity in the framework of Ziman's theory. We next develop an expression for the correction to be applied to the liquid's resistivity in order to account for the existence of a transient long-range

order, as assumed by Baiko *et al.*. The quantities other than ion structure factor which are required to calculate resistivity are provided by our INFERNO-based AA code PARADISIO [48]. We will show that satisfactory agreement with available experiments as well as with QMD theoretical results is obtained over a wide range of conditions ranging from solid state to plasma, by applying a single concept, consisting in correcting resistivities by removing the elastic contribution to the ion-ion structure factor.

The paper is organized in four parts. Sections II and III assemble the theoretical aspects of this work. Section II concerns the calculation of the electrical resistivity within Ziman's formulation and the average-atom picture. The calculation of the ion-ion structure factor is detailed in Sec. III. Section IV presents their application to aluminum, whereas our results are discussed in Sec. V.

II. THE ZIMAN FORMULATION OF ELECTRICAL RESISTIVITY IN THE FRAMEWORK OF THE AVERAGE-ATOM MODEL

Although this is not necessary under the thermodynamic conditions considered in this work, the following formulas will be given in the relativistic formalism for the sake of consistency with the relativistic average-atom code PARADISIO [48] that will be used to provide the needed inputs for resistivity calculations. We also will use atomic units (i.e., $e = \hbar = m_e = 1$).

The Ziman formulation of the electrical resistivity [30] describes, within the linear response theory, the acceleration of free electrons in a metal and their scattering by an ion. The resistivity reads then

$$\eta = -\frac{1}{3\pi Z^{*2}n_i} \int_0^\infty \frac{\partial f}{\partial \epsilon}(\epsilon, \mu) I(\epsilon) d\epsilon, \quad (2)$$

where n_i is the ion density and Z^* the mean ionic charge. The Fermi-Dirac distribution and its derivative read, respectively,

$$f(\epsilon, \mu) = \frac{1}{e^{\beta(\epsilon-\mu)} + 1} \quad (3)$$

and

$$\frac{\partial f}{\partial \epsilon}(\epsilon, \mu) = -\beta f(\epsilon, \mu)[1 - f(\epsilon, \mu)], \quad (4)$$

where $\beta = 1/(k_B T)$ and μ denotes the chemical potential. The function $I(\epsilon)$ is given by

$$I(\epsilon) = \int_0^{2k} q^3 S(q) \Sigma(q) dq, \quad (5)$$

where $S(q)$ denotes the static ion-ion structure factor and $\Sigma(q)$ the scattering cross section. The vector $\vec{q} = \vec{k}' - \vec{k}$ is the momentum transferred in the elastic scattering event (i.e., such as $|\vec{k}'| = |\vec{k}|$) of a conduction electron from an initial state \vec{k} to a final \vec{k}' one. Introducing the scattering angle $\theta \equiv (\vec{k}, \vec{k}')$ and its cosine $\chi = \cos \theta$, q^2 reads

$$q^2 = 2k^2(1 - \chi)$$

and

$$I(\epsilon) = 2k^4 \int_{-1}^1 S[k\sqrt{2(1-\chi)}] |a(k, \chi)|^2 (1-\chi) d\chi. \quad (6)$$

Energy ϵ and momentum k are related (within the relativistic formalism, c being the speed of light, and using atomic units) by

$$k = \sqrt{2\epsilon \left(1 + \frac{\epsilon}{2c^2}\right)}. \quad (7)$$

The t -matrix formalism of Evans [31] provides the electron-ion scattering amplitude $|a(k, \chi)|$, whose square is actually $\Sigma(q)$, given by, in the relativistic framework [28],

$$|a(k, \chi)|^2 = \frac{1}{k^2} \left(\left| \sum_{\kappa} |\kappa| e^{i\delta_{\kappa}(k)} \sin[\delta_{\kappa}(k)] P_{\ell}(\chi) \right|^2 + \left| \sum_{\kappa} \frac{|\kappa|}{i\kappa} e^{i\delta_{\kappa}(k)} \sin[\delta_{\kappa}(k)] P_{\ell}^1(\chi) \right|^2 \right), \quad (8)$$

where

$$\begin{aligned} \kappa &= -(\ell + 1) & \text{for } j &= \ell + 1/2, \\ \kappa &= \ell & \text{for } j &= \ell - 1/2. \end{aligned} \quad (9)$$

j and ℓ are the quantum numbers associated to the total angular momentum J and to the orbital momentum L , while P_{ℓ} and P_{ℓ}^1 denote respectively the Legendre and associated Legendre polynomials.

The average ion charge Z^* , chemical potential μ , and phase shifts $\delta_{\kappa}(k)$ needed in respectively Eqs. (2), (3), and (8), are obtained with the average-atom code PARADISIO [48], based on Liberman's atom-in-jellium model INFERNO [45]. The code handles all electronic states (bound and continuum ones) on an equal footing within the framework of quantum mechanics, which is an essential condition to correctly incorporate the effects of electron-electron interactions in the electron-ion phase shifts [49]. We recently applied it to the study of aluminum's thermal electronic properties [50] and showed its efficiency at low temperatures, where the atom-in-jellium approximation is often considered as too crude.

Since Z^* is not the average value of a quantum mechanical operator, it does not have a clear and unique definition. We give here three possible ones among the most widely used [51]. First, Z^* can be identified to the total number of continuum electrons,

$$Z_{\text{cont}} = \int_0^{\infty} f(\epsilon, \mu) X(\epsilon) d\epsilon, \quad (10)$$

where $X(\epsilon)$ denotes the continuum density of states, which includes not only electrons in the ideal (i.e., nonlocalized) states but also possible "quasibound" electrons in resonances. Alternatively, Z^* may be specified as the former free electrons alone

$$Z_{\text{free}} = \int_0^{\infty} f(\epsilon, \mu) X_{\text{ideal}}(\epsilon) d\epsilon, \quad (11)$$

where the ideal density of state reads, within the relativistic framework,

$$X_{\text{ideal}}(\epsilon) = \frac{k(1 + \epsilon/c^2)}{\pi^2 n_i}. \quad (12)$$

Actually, the ideal electron density is the one for $r \rightarrow \infty$, and so

$$Z_{\text{free}} = \left(\lim_{r \rightarrow \infty} n_e(r) \right) / n_i = \bar{\rho} / n_i. \quad (13)$$

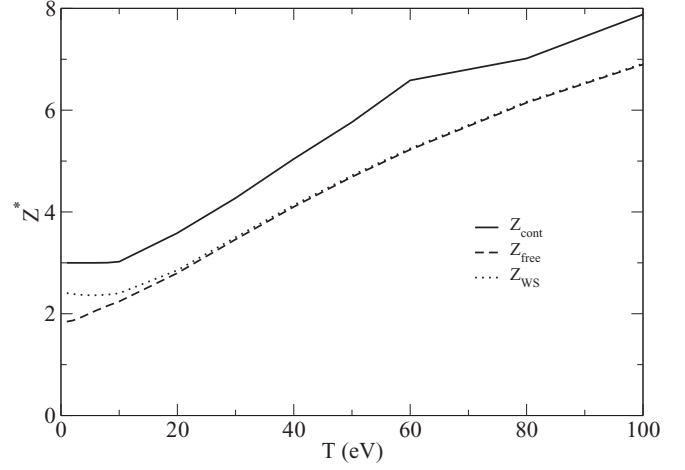


FIG. 1. Three possible definitions of the ion charge Z^* within ion-sphere models. Z_{cont} is the number of continuum electrons, Z_{free} denotes the ideally free electrons alone, and Z_{WS} corresponds to the charge on the Wigner-Seitz sphere. Case of aluminum at solid density.

Within the framework of the INFERNO model, $\bar{\rho}$ is the jellium density, i.e., the value of $n_e(r)$ at all radius $r > R_{\text{WS}}$, where

$$R_{\text{WS}} = (3/4\pi n_i)^{1/3} \quad (14)$$

denotes the radius of the Wigner-Seitz sphere. A third definition of Z^* involves the value of the electron density at the radius R_{WS} ,

$$Z_{\text{WS}} = n_e(R_{\text{WS}}) / n_i. \quad (15)$$

The equality of the three values is not obvious for AA models. However, in most situations, Z_{cont} , Z_{free} , and Z_{WS} are not so different and depart significantly from each other only in conditions favorable to pressure ionization, i.e., at high densities, and especially at low temperatures, when resonance states may notably be populated. Within the INFERNO model, this situation results in a sudden jump of the difference ($Z_{\text{WS}} - Z_{\text{free}}$). Figure 1 presents the case of aluminum at solid density ρ_0 . Since Z_{free} and Z_{WS} are close to each other for $300 \text{ K} \leq T \leq 100 \text{ eV}$, we retained $Z^* = Z_{\text{cont}}$ [Eq. (10)] as the definition of the mean ion charge, considering that the supplementary charge (typically one electron in the considered temperature range) contributes to electrical conductivity, although it is not ideally free.

III. ION-ION STRUCTURE FACTOR

A. Solid state case

Since the work of Baym [52], it is known that the formulation of the electrical resistivity of both liquids and solids stems from a same Ziman type expression where, for the solid, the phonon frequency weighted structure factor,

$$\bar{S}(\vec{k}) = \int \frac{\beta \hbar \omega}{1 - e^{-\beta \hbar \omega}} S(\vec{k}, \omega) d\omega, \quad (16)$$

is used, $S(\vec{k}, \omega)$ being the dynamic structure factor. At high-enough temperature (i.e., $\beta \hbar \omega \ll 1$), the weighting factors tend to unity, the integration over the frequencies yields the

static structure factor, and the familiar Ziman formula for the liquid is recovered. For crystalline solids at moderate temperatures, one of the main issues in calculating the resistivity is to perform the weighted integral accounting for absorption and emission of multiple phonons during the scattering process. Except for very low temperatures where the one-phonon (absorption or emission of a single phonon) processes dominate, the calculation of the weighted structure factor becomes rapidly intractable [53]. According to Rosenfeld and Stott [41], the difference between weighted $\bar{S}(\vec{k})$ and static $S(\vec{k})$ can be neglected for warm solids (i.e., for temperatures approaching melting one). Indeed, relying on a temperature expansion of the weighting factors, they found the difference varying as the inverse $1/m_i$ of the ion mass, from a maximum of 3% for lithium. They therefore assumed that $\bar{S}(\vec{k}) \simeq S(\vec{k})$ for these warm solids. Another important point in calculating the resistivity is how to deal with elastic (i.e., coherent or Bragg) scattering effects, which do not contribute. Taking advantage of a flexibility in Boltzmann equation, that allows to specify the density fluctuations entering the definition of $S(\vec{k})$ with respect to a reference configuration of ions, they prescribe the use of the effective structure factor,

$$S_{\text{eff}}(\vec{k}) = S(\vec{k}) - e^{-2W(k)} S_0(\vec{k}), \quad (17)$$

in Ziman formula for the calculation of solid's resistivity, where $S_0(\vec{k})$ is the static structure factor for the rigid perfect crystal, thermally damped by the Debye-Waller factor $e^{-2W(k)}$. W is related to the thermal mean-squared ion displacement $\langle u^2 \rangle_T$ by $W = \frac{k^2}{6} \langle u^2 \rangle_T$ [54]. Rosenfeld and Stott's approximation consists actually in subtracting the Bragg peaks with their full Debye-Waller weight, i.e., elastic scattering contributions, from the total multiphonon static structure factor, leaving only the inelastic contributions.

1. Multiphonon expansion for the static structure factor

In order to obtain the inelastic contributions to the static ion-ion structure factor $S(k)$, we applied Mangin *et al.*'s expansion [55] of the total structure factor as a sum of n -phonon factors $A_n(k)$,

$$S(k) = \left[A_0(k) + \sum_{n \geq 1} \frac{(2W)^n}{n!} A_n(k) \right] e^{-2W}. \quad (18)$$

$A_0(k)e^{-2W}$ is the elastic (i.e., zero-phonon) contribution to total $S(k)$, and the remaining terms constitute the inelastic n -phonon ($n \geq 1$) contributions. Within the Debye model of the density of phonon states, $2W$ reads [54]

$$2W(k) = \frac{3\hbar^2 k^2 T^2}{m_i k_B \theta_D^3} \int_0^{\theta_D/T} \left[\frac{1}{e^t - 1} + \frac{1}{2} \right] t dt, \quad (19)$$

where θ_D denotes the Debye temperature. For aluminum, $\theta_D = 428$ K from low temperature heat capacity measurements [56].

The Debye integral can be obtained analytically, using the following equality [57] involving the polylogarithm special

functions Li_n :

$$\begin{aligned} \frac{N}{x^N} \int_0^x \frac{t^N}{e^t - \alpha} dt \\ = \frac{N\Gamma(N+1)}{\alpha x^N} \left[\text{Li}_{N+1}(\alpha) - \sum_{i=0}^N \text{Li}_{N+1-i}(\alpha e^{-x}) \frac{x^i}{i!} \right], \end{aligned} \quad (20)$$

which gives, replacing both N and α by 1

$$\int_0^{\theta_D/T} \frac{t}{e^t - 1} dt = \frac{\pi^2}{6} - \text{Li}_2(e^{-\theta_D/T}) + \frac{\theta_D}{T} \ln(1 - e^{-\theta_D/T}), \quad (21)$$

where we have used the definition $\text{Li}_1(x) = -\ln(1-x)$ and the equalities $\text{Li}_2(1) = \pi^2/6$ and $\Gamma(2) = 1$. The dilogarithm function $\text{Li}_2(z)$ reads, for $|z| < 1$ ($z \in \mathbb{C}$),

$$\text{Li}_2(z) = \sum_{i=1}^{\infty} \frac{z^i}{i^2}. \quad (22)$$

Still applying the Debye model, the A_n functions are linked by a recursive relation,

$$A_n(\vec{k}) = \frac{\int_0^{q_D} q(2n_q + 1) dq \int A_{n-1}(\vec{k} + \vec{q}) d\Omega}{\int_0^{q_D} q(2n_q + 1) dq d\Omega}, \quad (23)$$

n_q denoting the phonon distribution function,

$$n_q = \frac{1}{e^{\frac{\theta_D}{T} \frac{q}{q_D}} - 1}, \quad (24)$$

where q_D reads

$$q_D = (6\pi^2 n_i)^{1/3}. \quad (25)$$

Calculation of the one-phonon function A_1 ,

$$A_1(\vec{k}) = \frac{\int_0^{q_D} q(2n_q + 1) dq \int A_0(\vec{k} + \vec{q}) d\Omega}{\int_0^{q_D} q(2n_q + 1) dq d\Omega}, \quad (26)$$

requires the elastic zero-phonon one. For a crystalline solid, it reads

$$A_0(\vec{k}) = \sum_{\vec{G}} \delta(\vec{k} - \vec{G}), \quad (27)$$

where the summation runs over reciprocal vectors \vec{G} . We have to calculate

$$A_0(\vec{k} + \vec{q}) = \sum_{\vec{G}} \delta(\vec{k} + \vec{q} - \vec{G}). \quad (28)$$

Gathering the reciprocal vectors in "layers" of $N(G)$ vectors of same length G ,

$$\sum_{\vec{G}} \delta(\vec{k} + \vec{q} - \vec{G}) = \sum_G N(G) \delta(|\vec{k} + \vec{q}|^2 - G^2), \quad (29)$$

leads to

$$\int A_0(\vec{k} + \vec{q}) d\Omega = \sum_G N(G) \int_{-1}^1 \delta(k^2 + q^2 + 2kq\chi - G^2) d\chi, \quad (30)$$

and finally to

$$A_1(k) = \frac{\int_0^{q_D} (2n_q+1)qdq \sum_G N(G) \int_{-1}^1 \delta(k^2+q^2+2kq\chi-G^2)d\chi}{4\pi \int_0^{q_D} (2n_q+1)qdq}. \quad (31)$$

Replacing $d\Omega$ by $-2\pi d\chi$, where $\chi = \cos\theta$, also in Eq. (23) one gets

$$A_n(k) = \frac{\int_0^{q_D} (2n_q+1)qdq \int_{-1}^1 A_{n-1}(k^2+q^2+2kq\chi)d\chi}{2 \int_0^{q_D} (2n_q+1)qdq}. \quad (32)$$

Solid aluminum at normal density $\rho_0 = 2.7 \text{ g/cm}^3$ crystallizes in the fcc structure. The Appendix gives the 10 first “layers” of reciprocal vectors \vec{G} . At normal density $q_D = 0.8$, $2k_F = 1.85$, and $2\pi/a = 0.821$ (atomic units), a denoting the fcc lattice parameter. The sum over the \vec{G} vectors must at least include the rows of length such as $G \leq 2k_F + q_D = 2.65$ a.u., i.e., the three first rows of reciprocal vectors.

Mangin *et al.* describe three approximations for the functions $A_n(k)$ among which the Meisel-Cote-Debye [58,59] one, believed to be the most appropriate for resistivity calculations.

2. The Meisel-Cote-Debye approximation

This approximation assumes that all the $A_n(k)$ functions with $n \geq 2$ are equal to $A_1(k)$,

$$A_1(k) = A_2(k) = \dots = A(k), \quad (33)$$

$A_1(k)$ being the only one function that has to be calculated. The total structure factor reads then

$$S(k) = A_1(k) + [A_0(k) - A_1(k)]e^{-2W}. \quad (34)$$

Since $A_0(k)e^{-2W}$ is the elastic contribution, the inelastic one is given by

$$S_{\text{inel}}^{(1)}(k) = A_1(k)(1 - e^{-2W}), \quad (35)$$

where the superscript means that only the $A_1(k)$ has been calculated. This approximation is certainly a good one if the weights of the zero-phonon and the one-phonon contributions are the largest, which is the case at very low temperature and low k but could be poor close to melting. We therefore propose to determine as much A_n terms as needed to obtain converged $S(k)$ for k up to $2k_F$ and temperature up to melting.

The inelastic structure factors $S_{\text{inel}}^{(n)}(k)$, where the superscript (n) means that $i = 0 \dots n$ $A_i(k)$ terms are exactly computed using Eq. (32) and the $i > n$ $A_i(k)$ functions are taken equal to the last calculated $A_n(k)$, are related by the following recursive equation:

$$S_{\text{inel}}^{(n)}(k) - S_{\text{inel}}^{(n-1)}(k) = [A_n(k) - A_{n-1}(k)] \left[1 - e^{-2W} \sum_{i=0}^{n-1} \frac{(2W)^i}{i!} \right]. \quad (36)$$

We consider that convergence is achieved when

$$\int_0^{2k_F} \left[\frac{S_{\text{inel}}^{(n)}(k) - S_{\text{inel}}^{(n-1)}(k)}{S_{\text{inel}}^{(n)}(k)} \right]^2 dk \leq 10^{-6}, \quad (37)$$

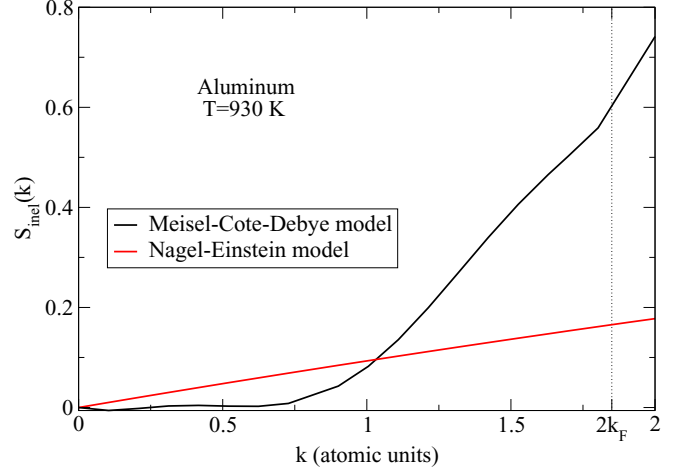


FIG. 2. Inelastic structure factor for solid aluminum at $T = 930$ K (i.e., closed to melting). The black curve is obtained applying the Meisel-Cote-Debye approximation [58,59] taking into account scattering processes involving up to five phonons. The red one corresponds to the simpler Nagel-Einstein one [60].

which is the case with only $n = 5$ terms exactly computed for normal density aluminum at melting temperature $T = 930$ K and $n = 3$ at ambient one $T = 300$ K. Figure 2 presents, in black, the inelastic structure factor obtained for solid aluminum at temperature close to melting, when the Meisel-Cote-Debye approximation is applied. The dashed vertical line marks the upper $2k_F$ limit for the q momentum transferred in the scattering process. The figure also shows another, however crude, possible approximation, i.e., the Nagel-Einstein [60] one, presented in Mangin *et al.*’s paper. In this extreme model, all the $A_n(k)$ ($n \geq 1$) are taken equal to 1, which leads to the following inelastic structure factor:

$$S_{\text{inel}}^{\text{NE}} = 1 - e^{-2W}. \quad (38)$$

This corresponds to the choice made in Ref. [44] for the inelastic part of the structure factor. The Meisel-Cote-Debye approximation provides a more realistic ion-ion structure factor with a limited computational cost since only a small number of the $A_n(k)$ functions have to be calculated.

B. Liquid state case

Baiko *et al.*’s assumption relies on numerical simulations from different authors (the example of the molecular-dynamics study of Schmidt *et al.* [61] is cited) which suggest that there is a temporary long-range order at coupling parameter $\Gamma \gg 1$ [Γ is defined in Eq. (47)]. According to the authors, this long-range order may be preserved during typical electron scattering time, giving rise to a temporary electron band structure and an associated temporary elastic scattering whose effect on the electric resistivity has to be removed, as in the solid state. Following this idea, the total structure factor $S(q)$ for the liquid must be replaced in Ziman formula by

$$S_{\text{inel}}(k) = S_{\text{tot}}(k) - S_{\text{el}}(k). \quad (39)$$

According to Mangin *et al.* [55],

$$S_{\text{el}}(k) = A_0(k)e^{-2W(k)} = \sum_G N(G)\delta(k-G)e^{-2W(k)}. \quad (40)$$

In the present work, we use the total structure factor $S_{\text{tot}}(k)$ obtained by solving the hypernetted-chain (HNC) equations for charged spheres [62]. The semiempirical correlation function $g(r)$ from Held and Pignolet [63] is used to initialize the iteration process.

Subtracting the elastic contribution $S_{\text{el}}(k)$ results to the following effect on the electric resistivity:

$$\eta = \eta_{\text{tot}} - \delta\eta_{\text{el}}, \quad (41)$$

where η_{tot} is the resistivity obtained with the total structure factor and $\delta\eta_{\text{el}}$ the correction,

$$\delta\eta_{\text{el}} = \frac{1}{3\pi Z^{*2} n_i} \int_0^\infty \left(-\frac{\partial f}{\partial \epsilon} \right) I_{\text{el}}(\epsilon) d\epsilon. \quad (42)$$

Using Eq. (40)

$$I_{\text{el}}(\epsilon) = \int_0^{2k} q^3 S_{\text{el}}(q) \Sigma(q) dq = \sum_G N(G) e^{-2W(G)} \times 2k^4 \int_{-1}^1 (1-\chi) |a(k, \chi)|^2 \delta[G - k\sqrt{2(1-\chi)}] d\chi, \quad (43)$$

and

$$\delta\eta_{\text{el}} = \frac{1}{3\pi Z^{*2} n_i} \sum_G N(G) e^{-2W(G)} \times \int_{G/2}^\infty \left(-\frac{\partial f}{\partial k} \right) 2k^4 \frac{G^2}{2k^2} \times \left| a\left(k, 1 - \frac{G^2}{2k^2}\right) \right|^2 dk. \quad (44)$$

For the solid, the Debye-Waller factor $e^{-2W(k)}$ was calculated within the Debye model for phonon density of states. For the present liquid case, we used an analytic fit proposed by Baiko and Yakovlev [64], also given in Ref. [43],

$$W(k) = \alpha_1 (u_{-1} e^{-9.1\tau} + 2\tau u_{-2}) / 4. \quad (45)$$

$u_n = \langle (\omega/\omega_{pi})^n \rangle_{\text{ph}}$ is a frequency moment where $\omega_{pi} = (4\pi Z^{*2} n_i / m_i)^{1/2}$ designs the ion plasma frequency. The brackets $\langle \dots \rangle_{\text{ph}}$ mean an average over phonon frequencies ω . From Ref. [65], $u_{-1} = 2.8$ and $u_{-2} = 13$ for body-centered cubic (bcc) lattices. We rely on Potekhin *et al.*'s assertion [43] that the effective structure factors for fcc lattices are almost indistinct from those for bcc one, to also use these values in our calculations assuming a fcc temporary long-range order in liquid aluminum. Parameter τ reads $\tau = T/T_p$ with $T_p = \hbar\omega_{pi}/k_B$ (i.e., ω_{pi} in the atomic units used in this paper) denoting the ion plasma temperature, and

$$\alpha_1 = \alpha_0 \frac{k^2}{4k_F^2}, \quad \text{with } \alpha_0 = \frac{4k_F^2 R_{\text{WS}}^2}{3\Gamma\tau}, \quad (46)$$

and where

$$\Gamma = \frac{Z^{*2}}{(k_B T) R_{\text{WS}}} \quad (47)$$

is the plasma ionic coupling parameter, here given in atomic units, and we recall that $R_{\text{WS}} = (3/4\pi n_i)^{1/3}$ denotes the Wigner-Seitz sphere radius.

This expression for $W(k)$ is fitted to calculations for densities from 10^3 to 10^{11} g/cm³ and totally ionized plasmas, but is expected, according to Refs. [43,64], to be applicable at lower

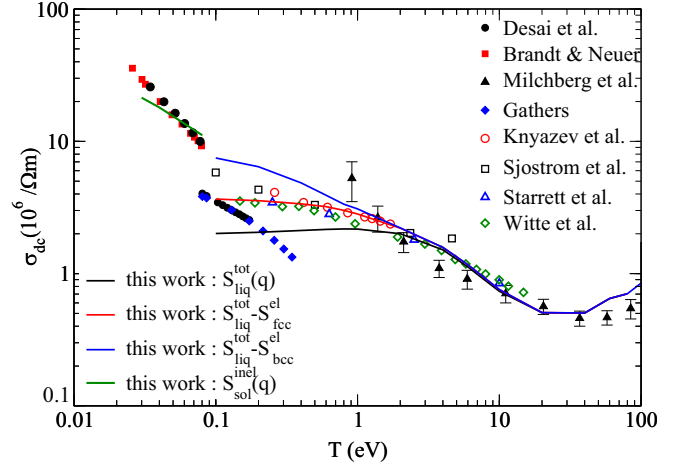


FIG. 3. Isochoric $\rho = 2.7$ g/cm³ aluminum's electrical conductivities. Filled symbols: Experiments, from Desai *et al.* [14] (black filled circles), Brandt and Neuf [15] (red filled squares), Gathers [16] (blue filled diamonds), and Milchberg *et al.* [13] (black filled triangles). Empty symbols: Molecular-dynamics results, from Knyazev *et al.* [17] (red empty circles), Sjostrom *et al.* [18] (black squares), Starrett *et al.* [19] (blue triangles), and Witte *et al.* [20] (green diamonds). Lines: Our results. Black line: Using total HNC $S(q)$. Red and blue lines: Elastic contributions have been subtracted from $S(q)$, assuming respectively fcc and bcc long-range order in liquid aluminum.

densities down to 1 g/cm³, if we use the effective ion charge in the relations (instead of the atomic number Z).

IV. RESULTS

As already underlined in the Introduction, aluminum has been the subject of a large number of experiments and theoretical studies, covering a wide range of temperatures from ambient one up to typically 100 eV, at densities close to normal $\rho_0 = 2.7$ g/cm³ one. QMD works provide an isochoric ($\rho = \rho_0$) set of electrical conductivities. Experimental values are mostly from isobaric techniques, and give the opportunity to investigate slightly lower densities. Recently, ultrafast heating methods [12] allowed to experiment in conditions where only the electronic component of the matter is heated while ions remain cold, giving the possibility to extend the temperature range for which correcting the ion-ion structure factor from elastic contributions could be necessary. These conditions have been studied theoretically by Dharma-wardana *et al.* [39], resulting in predictions for electronic temperatures up to $T_e \approx 10$ eV, that can be used to complete Sperling *et al.*'s few experiments. Additionally, experimental resistivities are also well documented for solid aluminum. They provide an opportunity to assess the relevance of our atom-in-jellium approach for the solid state.

A. Isochoric average-atom conductivities

Figure 3 displays most of the experimental (filled symbols) and theoretical (empty symbols) electrical conductivities available for dense aluminum, at temperatures $300 \text{ K} \leq T \leq 100 \text{ eV}$. For solid aluminum ($T \leq T_{\text{melt}} \approx 930 \text{ K}$), experimental values are taken from Desai *et al.*'s compila-

tion [14] of numerous data (black filled circles) and from Brandt and Neuer's paper [15] (red filled squares). For liquid aluminum, values from Desai *et al.* [14] (black filled circles above typically 0.1 eV) and from Gathers [16] (blue filled diamonds) are reported. The latter correspond to the values given in column 5 of Gathers's Table II, and extend Desai *et al.*'s one in the liquid domain. As pointed out by several authors [20,21,39], all these data are density corrected and fall under isobaric conditions and not under isochoric ones. Gathers's liquid aluminum values correspond to densities from 2.4 g/cm³ to 1.7 g/cm³. For solid aluminum, density deviations from normal ρ_0 one are less important. Leitner *et al.* [66] report the value $\rho = 2.514$ g/cm³ just before melting, i.e., only 7% less than ρ_0 , so that we retained these solid-state experimental conductivities for comparisons to our isochoric calculations. The case of Gathers's isobaric conductivities will be considered in a next section. Above the highest temperature reported by Gathers, some of the Milchberg *et al.*'s experimental results [13] from isochoric laser heating (black filled triangles with error bars) are also presented.

Empty symbols correspond to theoretical results obtained for $\rho_0 = 2.7$ g/cm³, mainly with the use of QMD associated to Kubo-Greenwood approximation. Red empty circles are from Knyazev *et al.*'s paper [17], green empty diamond from Witte *et al.*'s one [20] and blue empty triangles from Starrett *et al.*'s work [19]. Empty black squares are taken from Sjostrom *et al.*'s one [18], which differs from the preceding studies by the use of orbital-free molecular-dynamics.

The curves correspond to our Ziman-Evans calculations for aluminum at normal density using quantities from the AA code PARADISIO.

For solid aluminum ($T \lesssim 0.08$ eV) the agreement between our calculations at ρ_0 (green solid line) and the experiments (black and red solid circles) is rather satisfactory. The observed differences can be explained. Near melting, they are consistent with the fact that the actual experimental densities differ slightly from ρ_0 . Just before melting, we obtained $\sigma = 11.12$ ($\mu\Omega\text{m}$)⁻¹ instead of 9.46 ($\mu\Omega\text{m}$)⁻¹ experimentally. As specified a little above, Leitner *et al.* [66] estimate a 7% reduction of the density near melting. Since $\sigma \propto 1/n_i \propto 1/\rho$, a crude correction for deviation to normal density would lead to a "corrected" value $\sigma_{\text{correc}} \approx 10.34$ ($\mu\Omega\text{m}$)⁻¹ which approaches the experiment. At ambient temperature, where experimental density is ρ_0 , the observed discrepancies may reflect the fact that, at low temperature ($T \ll \Theta_D$), the weighted $\bar{S}(k)$ structure factor no more reduces to static $S(k)$ one. Since Mangin *et al.*'s expression is an unweighted integration of the dynamic structure factor, its use for the calculation of the resistivity is questionable at temperatures $T \ll \Theta_D$.

Three results are presented for temperatures above melting ($T \gtrsim 0.08$ eV). The black curve was obtained using total HNC ion-ion structure factor, and the red and blue ones applying the correction $\delta\eta_{ei}$ [Eq. (42)] that accounts for transitory long-range order in the liquid. Removing these latter effects has clearly an incidence on our theoretical electrical conductivities. Furthermore, the conductivities are sensitive to the type of long-range order. The red curve corresponds to fcc one while the blue curve describes the effect of a bcc one. We consider the fact that the red curve obtained with fcc order, which is solid aluminum's crystallographic form at normal

density, is in better agreement with most of the available other theoretical results than the blue curve (bcc long-range order) as an encouraging result. However, just above melting, the red curve seems too low compared to Gathers's experiments [16], given the fact that they relate to liquid densities, and are therefore themselves lower than normal density conductivities. On the other hand, the blue curve, once the density effects have been corrected, could better match the experiments. This hypothesis will be examined below (Sec. IV B).

Figure 4 focuses on liquid and plasma states and presents conductivities on a linear scale. Experimental values from Gathers [16] and Milchberg *et al.* [13] as well as molecular-dynamics results [17–20] already shown in Fig. 3 are repeated and completed by other theoretical conductivities. Sperling *et al.*'s results [67] are represented by the blue dot-dot-dashed line and Shaffer and Starrett's ones [68] by the black short dashes. Witte *et al.*'s results presented in Fig. 3 (green diamonds) are relative to calculations using Perdew-Burke-Ernzerhof (PBE) approximation for exchange-correlation (XC) functional [69] in the framework of the generalized-gradient-approximation (GGA). Figure 4 also presents (magenta down-triangles) the same authors's results based on the GGA Heyd-Scuseria-Ernzerhof (HSE) XC functional [70] and QMD calculations of Dharma-wardana *et al.* [39] (red right-triangles) also based on PBE XC functional. Sjostrom *et al.* (red circles) and Knyazev *et al.* (black squares) used the local-density-approximation (LDA) Perdew-Zunger (PZ) XC functional [71], and Starrett *et al.* [19] the GGA-PBE one. We can note that that all GGA-PBE- and GGA-HSE-based values are close each to other and it is the same for LDA-based calculations. LDA XC functionals predict higher conductivities than GGA ones, among which HSE XC functional leads to lower values than PBE. Our own results (red curve, assuming fcc long-range-order in liquid aluminum) stem from quantities obtained with our AA code PARADISIO, using Karasiev *et al.*'s LDA XC functional [72] and follow the same trends as the LDA works of Refs. [17,18], at least for $T \gtrsim 0.4$ eV. This observation strengthens our confidence in the reliability of our results.

The further curves present the results of others than QMD studies. Two AA calculations, standing on either side of our curve, are reported. Perrot and Dharma-wardana's work [37] (thin black dotted line) focuses on Milchberg *et al.*'s experiments above typically 20 eV. Good agreement with the latter was achieved using constant electron density $n_e = 0.027$ atomic units and $Z^* = Z_{\text{cont}}$. The dot-dashed green line presents Faussurier and Blancard's AA results for isochoric conductivity (i.e., constant n_i), with $Z^* = Z_{\text{WS}}$ for the ion charge [38]. The two calculations differ also by the ion-ion structure factor $S(k)$. Faussurier and Blancard used a simple analytic expression for the one-component plasma [73] one, whereas Perrot and Dharma-wardana solved the modified HNC (MHNC) equation, i.e., HNC including a bridge function [74]. This difference in the $S(k)$ may contribute to the strong discrepancies observed between the two curves at $T \lesssim 10$ eV. At higher temperature, the resistivity becomes less sensitive to $S(q)$, and the remaining divergences stem from different assumptions for charge densities.

The figure also presents Sperling *et al.*'s calculations [67] (blue dot-dot-dashed line). The authors used for $S(k)$ at

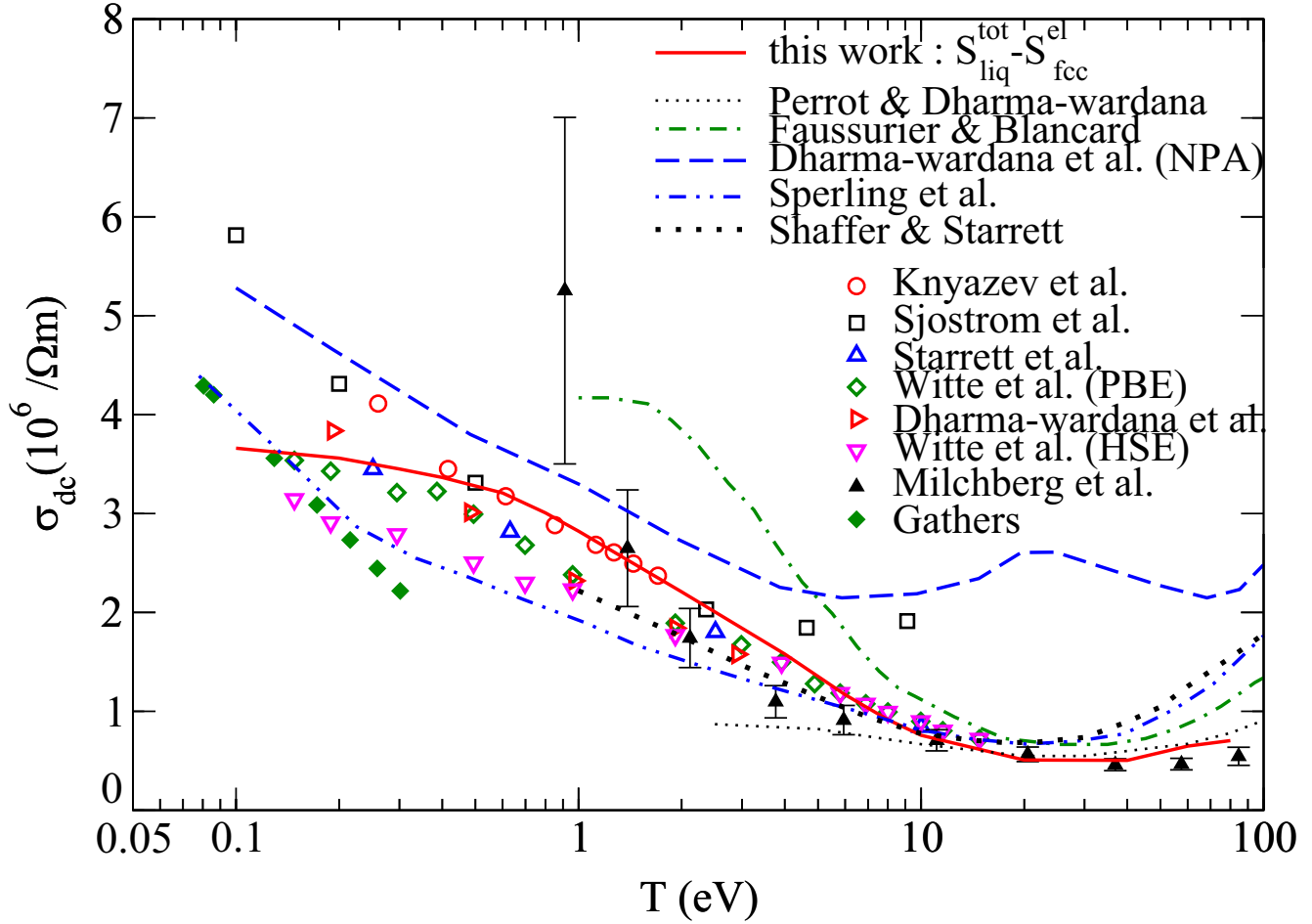


FIG. 4. The figure repeats the theoretical results presented in the preceding Fig. 3, focusing on the liquid and warm-dense-matter states, and completes them with some other calculations. Magenta down-triangles: Witte *et al.*, using another XC functional (i.e., HSE) [20]. Red right-triangles: QMD values from Dharma-wardana *et al.* [39]. Red line: Present work, subtracting elastic contributions to total HNC $S(q)$, assuming long-range fcc order in the liquid. Thin black dotted line: AA results from Perrot and Dharma-wardana [37]. Green dot-dashed curve: AA calculation from Faussurier and Blancard [38]. Blue dot-dot-dashed curve: From Sperling *et al.*'s work [67]; black short dashes: Shaffer and Starrett's recent work [68]; and blue dashed line: Neutral pseudoatom (NPA) calculation [39].

$0.08 \text{ eV} < T < 6 \text{ eV}$, an interpolation between the Percus-Yevick approximation, valid for the liquid state, and the classical-map hypernetted-chain one, applicable above 6 eV . They considered a four-parameter electron-ion pseudopotential, two of them weighting long-range Coulomb potential and Pauli repulsion and being temperature dependent through an additional variable noted a . Measured phonon dispersion curves at melting point are used to obtain all values, at the exception of a which remains adjustable. The figure presents results obtained with $a = 2$, which is close to the expected $a \approx \pi^2/4 \approx 2.47$ value estimated within LDA. The curve follows closely the first Gathers's raw points, i.e., derived from the measured electrical resistances and not yet corrected from thermal expansion (more details on Gathers's experiments will be given in Sec. IV B).

The black short dashes correspond to the recent calculation of Shaffer and Starrett [68] combining quantum Landau-Fokker-Planck equation with the concept of mean-force scattering, whose results are close to Witte *et al.*'s QMD ones.

To complete this overview, we also report the very different results obtained by Dharma-wardana *et al.* [39] with

the neutral pseudoatom (NPA) method. While most AA models, among which those based on Liberman's INFERNO one, confine the electrons inside the ion sphere, neutral-pseudoatom method widens this border for free electrons to a "correlation sphere," whose radius is large enough that all correlations with the central ion vanish at the surface of this sphere. The most important outcomes are the removal of the ambiguity on the definition of the ion charge Z^* , and the improved description of the free electronic states and of the ionization processes. This changes drastically the shape of the conductivity at high temperature, especially in the range where Milchberg *et al.*'s experiments show a minimum of the conductivity, compared to customary AA results. The blue dashed curve corresponding to the NPA results presents, instead of that, a minimum conductivity close to 6 eV , followed by a maximum in the vicinity of 25 eV , and, finally, a second minimum near 70 eV , resulting from the competition between different ionization states, which is, according to the authors, out of the scope of ion sphere AA methods. This zone of the minimum conductivity (maximum resistivity) has been the subject of a number of studies [37,39,68,75,76], leading to

TABLE I. Aluminum densities relative to Gathers's isobaric resistivities.

T (K)	933	1000	1500	2000	2500	3000	3500	4000
ρ (g/cm ³)	2.42	2.41	2.29	2.18	2.08	1.97	1.87	1.77

different interpretations. In Sec. IV C, we will retain the fact, mentioned in Ref. [76], that Milchberg *et al.*'s experiments should be analyzed with a two-temperature formalism.

We presented, in this section, electrical conductivity calculations for solid density aluminum covering a wide range of conditions from solid state to plasma. The same HNC structure factor was used from the liquid to the plasma, there where other works used interpolations between two limiting approximations. It is the case, for instance, for Sperling *et al.*'s work where $S(k)$ interpolates between HNC structure factor, relevant for plasmas, and Percus-Yevick one, often applied to liquids. In our work, the agreement with both experiments and QMD data is the result of the subtraction of elastic contributions to $S(k)$, a concept first developed for solid-state resistivity, here extended above melting.

B. Isobaric conductivities

Gathers experimental values for liquid aluminum's isobaric resistivities are reported in Table II of his paper [16]. Two sets of data are given in columns 4 and 5. Indeed, because of the important scatter in the measured volumes, the author first calculated resistivities using resistance ratio and the fixed *room temperature* geometry for each shot. These raw values are noted as ρ_e^* , and fitted by Gathers's Eq. (9). Gathers obtained afterwards the actual isobaric resistivities, corrected from thermal expansion, and noted as ρ_e , by multiplying his Eq. (9) by his Eq. (7) which fits the volume expansion ratio v/v_0 . The results are finally fitted by his Eq. (8) in the range of overlap. It seems that there is a misprint in the labeling of columns 4 and 5 of Gathers's Table II. It is easy to verify that the values of column 4 (labelled as ρ_e) correspond to Gathers's Eq. (9), i.e., to the raw uncorrected ρ_e^* resistivities, and those of column 5 (labelled as ρ_e^*) to Eq. (8), i.e., the actual experimental resistivities ρ_e , resulting from the correction for thermal expansion of the ρ_e^* 's. We therefore believe that the blue diamonds corresponding to the data of column 5 are the true isobaric conductivities, joining this way Witte *et al.*'s point of view.

Our calculations are represented by the full and dashed lines in Fig. 5, where the continuous ones recall the results obtained for the isochore $\rho = \rho_0$ considering transient fcc (the lowest continuous red curve) or bcc (the highest continuous blue one) order in liquid aluminum. The dashed lines are their counterparts for the densities and temperatures given in Table I. These two curves frame the experimental values. The lowest red dashed line obtained assuming fcc-like order is closest to experimental conductivities. Actually, retaining fcc or bcc-like order is somewhat arbitrary, although the fcc hypothesis is consistent with solid aluminum's crystallographic structure. However, both fcc and bcc can be seen as particular tetragonal-centered structures, with respectively $c/a = 1$ and $c/a = 1/\sqrt{2}$ ratios. A slight compression of the fcc cell along vertical c axis in our calculations would certainly improve the

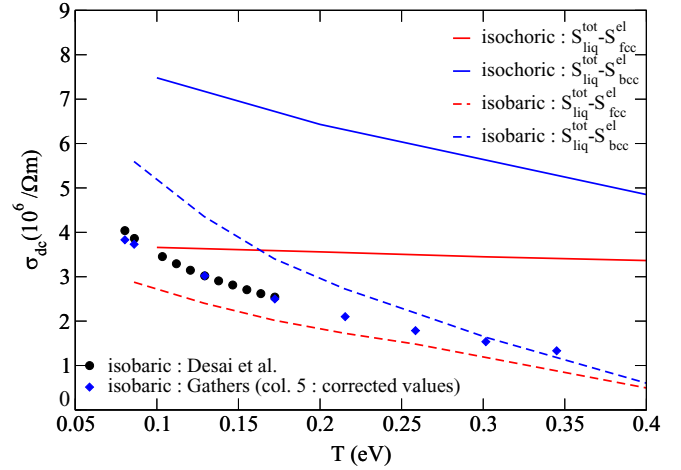


FIG. 5. Isobaric electrical conductivity for liquid aluminum. Blue diamonds: Experiments from Table II (column 5: Final data after correction from thermal expansion) of Ref. [16], and black circles: Desai *et al.*'s values. Our previous isochoric results are recalled by the continuous red and blue curves. Dashed curves: Our AA isobaric conductivities, assuming fcc long-range order in the liquid (the lowest red dashed line) and bcc one (the highest blue dashes).

agreement with the experiments. Our aim was here to check the ability of our approach, i.e., correcting resistivities from these effects, to predict also isobaric values. This is clearly the case, within the uncertainty on the actual transient long-range order in liquid aluminum.

C. Two-temperature conductivities

Sperling *et al.* measured surprisingly low electrical conductivities for solid density aluminum at $T \approx 0.2$ eV and $T \approx 6$ eV, using the Linac Coherent Light Source (LCLS) facility [12]. The LCLS experiments are interpreted in Ref. [39] as ultrafast ones, where the sample is heated and probed on a timescale short enough to keep the ions at some temperature $T_i = T_0$ while electrons are heated up to $T_e \gg T_i$. For similar reasons, Milchberg *et al.*'s experiments [13] using short laser pulses are also considered to belong to this category of ultrafast methods [76]. Indeed, a two-temperature extension of Ziman's expression for electrical resistivity, assuming $T_0 = 0.06$ eV accounts satisfactorily for Sperling *et al.*'s values [77]. The latter correspond to the red squares of Fig. 6, and the black triangles in the same figure represent Milchberg *et al.*'s electrical conductivities, here rescaled by Dharma-wardana and Perrot [76]. Actually, Milchberg *et al.* did not measure the temperature but estimated it according to a $Z^*(T)$ theoretical relation. In the figure, the triangles are somewhat horizontally shifted compared to the preceding figures, according to Dharma-wardana and Perrot's temperature reevaluation, based on their own ion charges Z^* . The lines correspond to the theoretical conductivities. The black dashed curve represents NPA results from Ref. [39] at $0.1 \text{ eV} \lesssim T_e \lesssim 10 \text{ eV}$, which lie substantially below their $T_i = T_e$ counterparts. It is unfortunate that there is no calculation above 10 eV, but we can guess that a similar down shift of the $T_i = T_e$ curve of the Fig. 4 occurs, probably resulting in a curve slightly oscillating among Milchberg *et al.*'s points. Earlier two-temperature

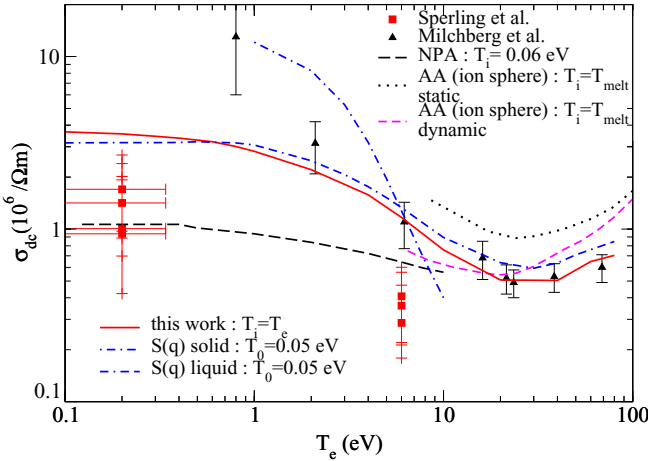


FIG. 6. Fast-heated aluminum's electrical conductivity. Red squares: x-Ray heating using the LCLS facility [12], and black triangles: Laser heating from Milchberg *et al.* [13], reconsidered by Dharma-wardana and Perrot [76]. Long black dashes: Two-temperature NPA results, at $0.1 \text{ eV} \lesssim T_e \lesssim 10 \text{ eV}$. Short black dashes: Two-temperature ion-sphere static conductivity, and magenta dashes: Two-temperature ion-sphere dynamic conductivity $\sigma(\omega)$, with $\hbar\omega = 4.026 \text{ eV}$. Red continuous line: This work, with $T_e = T_i$. Our two-temperature conductivities: Use of the solid state $S(q)$ (blue dot-double-dashed) and liquid state one (blue double dot-dashed line) at ion temperature $T_0 = 0.05 \text{ eV}$.

AA-based studies from Dharma-wardana and Perrot [76] are however available for $T \gtrsim 10 \text{ eV}$, and represented by the black short dashes and magenta dots. The black dashes correspond to static two-temperature electrical conductivity. The authors of Ref. [76] obtained better agreement with the experiments with dynamic two-temperature conductivity $\sigma(\omega)$ (magenta dashes), where $\hbar\omega = 4.026 \text{ eV}$, the laser wavelength being $\lambda = 308 \text{ nm}$. This last curve almost connects to the NPA calculations in the vicinity of $T_e \approx 10 \text{ eV}$, despite the use of a less sophisticated AA method.

The continuous red curve of Fig. 6 recalls our isochoric conductivities. The blue dot-double-dashed line corresponds to our two-temperature calculations, using two-temperature Ziman formalism.

In the latter, the resistivity reads [76,78]

$$\eta_{2T} = -\frac{1}{3\pi} \frac{n_i(T_i)}{n_e(T_e)^2} \int_0^\infty \frac{\partial f}{\partial \epsilon}(\epsilon, \mu, T_e) I(\epsilon, T_i, T_e) d\epsilon, \quad (48)$$

the electron density at T_e and the ion density at T_i being related by

$$n_e(T_e) = Z^* n_i(T_i). \quad (49)$$

The two-temperature integral $I(\epsilon, T_i, T_e)$ is given by

$$I(\epsilon, T_i, T_e) = \int_0^{2k} q^3 S(q, T_i, T_e) \Sigma(q, T_e) dq. \quad (50)$$

Fermi distribution function and scattering cross section are here respectively denoted by $f(\epsilon, \mu, T_e) \equiv f(\epsilon, \mu(T_e))$ and $\Sigma(q, T_e)$ to recall that these functions are relative to electrons at temperature $T_e \neq T_i$. In the same way, $S(q)$ is here replaced by $S(q, T_i, T_e)$, i.e., the structure factor for an assem-

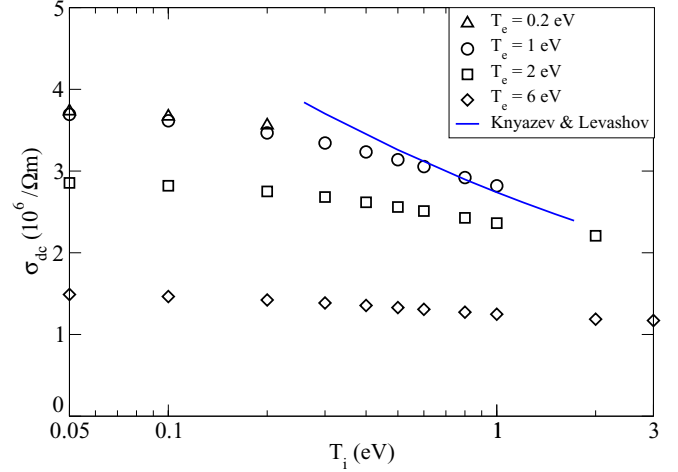


FIG. 7. Two-temperature aluminum's electrical conductivities, assuming a liquid structure factor $S(q, T_i)$ at different temperatures T_i (symbols). The blue line is an approximation of Knyazev and Levashov's QMD results for $3000 \text{ K} \leq T_i \leq T_e \leq 20\,000 \text{ K}$ [79].

bly of ions at temperature T_i immersed in an electron gas at temperature T_e .

In the analysis of ultrafast experiments, it is considered that the sample is preheated to some temperature T_0 , which constitutes the initial sample temperature before heating by the main pulse. The ion-ion structure factor used for the calculation of the two-temperature resistivity is therefore $S(q, T_0, T_0) \equiv S(q, T_0)$. Furthermore, Petrov *et al.* [78] rely on their observation that the interactions depend weakly on the electron temperature in the case of aluminum, to justify the use of the same $S(q, T_0)$ structure factor.

These authors investigated the variation in electrical resistivity with both T_i and T_e . Applying the two-temperature Ziman expression, they found that the resistivity decreases when the ion temperature T_i is lowered. Knyazev and Levashov observe the same trend with QMD-KG approach and propose the following approximation [79] of their results for $3000 \text{ K} \leq T_i \leq T_e \leq 20\,000 \text{ K}$:

$$\sigma_{\text{KL}}(T_i, T_e) = \frac{2.844 \cdot 10^7}{[T_i(\text{K})]^{0.25}} \Omega^{-1} \text{ m}^{-1}. \quad (51)$$

These results exclude the possibility of notable preheating of the aluminum sample up to liquid state in LCLS experiments, and join the conclusion of the two-temperature calculations presented in Ref. [39] using a liquid structure factor $S(q, T_0)$, with $T_0 = T_{\text{melt}}$. We report, in Fig. 7, some two-temperature conductivities $\sigma(T_i, T_e)$ for a few values of electron temperature, including those $T_e = 0.2 \text{ eV}$ and $T_e = 6 \text{ eV}$ corresponding to the LCLS experiments, the ion temperatures varying in the range $0.05 \text{ eV} \leq T_i \leq 3 \text{ eV}$ (symbols), that supports this conclusion. The resistivities are calculated as described in Sec. III B, i.e., subtracting the elastic contribution $\delta\eta_{\text{el}}$ from the two-temperature resistivities obtained with the HNC structure factors $S(q, T_i)$. The agreement of our results with Knyazev and Levashov's QMD two-temperature conductivities [approximated by Eq. (51) and illustrated in Fig. 6 by the blue line] in the range $0.3 \text{ eV} \lesssim T_i \leq T_e \lesssim 1 \text{ eV}$, only observed when the correction $\delta\eta_{\text{el}}$ to the liquid's

resistivity is applied, is an argument in favor of the relevance of our approach for two-temperature calculations, too.

Since we obtained satisfactory results in the solid-state domain with the structure factor derived using Meisel-Cote-Debye approximation, we used it for the calculation of two-temperature conductivities and obtained the blue dot-single-dashed curve of Fig. 6, which is in qualitative agreement with Milchberg *et al.*'s laser heating experiments for $T_e < 10$ eV, but well above the LCLS conductivities. This suggests that the state of aluminum before the main heating in LCLS experiments probably is neither a perfect liquid nor a perfect solid. Indeed, the black dashed curve of Fig. 6 was obtained by Dharma-wardana *et al.* using an ion-ion structure factor that corresponds to a "supercooled" liquid at temperature $T_0 = 0.06$ eV [39]. Built to mimic the solid's spherically averaged structure factor, it combines a pseudopotential capable, according to the authors, to account accurately for solid-state properties like phonons dispersion curves, to the MHNC equations describing the pair correlations in a fluid.

To some extent, we have, in this section, shown the relevance of our approach in the conditions of ultrafast experiments, where electrons are heated up to temperatures T_e higher than ion ones T_i . Milchberg *et al.*'s electrical conductivities at $T_e \lesssim 10$ eV are explained assuming there is limited preheating before the main laser pulse, the ion subsystem remaining in the solid state. As electron temperature rises above 10 eV, the agreement with Milchberg *et al.*'s points can be reached considering progressive preheating to liquid state. Concerning x-ray heating in LCLS experiments, we agree with Dharma-wardana *et al.* when we conclude that the initial state before main heating can not be a normal liquid (i.e., a liquid at temperature above melting). However, we believe that it can neither be solid. Dharma-wardana *et al.* obtained nevertheless satisfactory agreement with the experiments assuming a "supercooled" liquid initial state but not solid. A similar calculation is, at the present time, out of our scope. The use of Held and Pignolet's semiempirical ion-ion pair potential with HNC equations reaches here its limits. A more realistic pair potential should be constructed in close connection with our AA code for that purpose.

V. CONCLUSION

We presented a calculation of dense aluminum's electrical conductivity from the solid state to the hot plasma within Ziman's formulation. The latter theory requires the knowledge of ion-ion structure factors, for which several approximations are available, more or less relevant for each given domain of density and temperature. The resolution of the hypernetted-chain equations for charged spheres gives satisfactory results for the plasma, but Percus-Yevick approximation is often preferred for the liquid state. The question of how to fill the gap between these two limits then arises. Recently, our attention was caught by the encouraging results obtained in Ovechkin *et al.* and Hansen *et al.*'s works where a widely accepted point of view for the solid state, consisting in retaining only the inelastic part of the structure factor for resistivity calculation with Ziman's formula, is extended to the liquid state. In the present work, we have pushed this approach further, in order to obtain continuity in the ion-ion structure factors, from solid to plasma states.

Ovechkin *et al.* do not consider the solid-state case, and Hansen *et al.* apply Baiko *et al.*'s model for solid ion-ion structure factor. In the present work we computed the multiphonon expansion for the solid's structure factor. The inelastic part corresponds to the terms including at least one phonon in the pair interaction. We obtained converged inelastic structure factor including up to the fifth term, i.e., the one involving creation and/or destruction of five phonons. Except the value of the Debye-Waller factor damping the Bragg peaks in the elastic part (zero-phonon term in the multiphonon expansion of the structure factor) required for the solid phase, all other quantities can be obtained from our average-atom code, including the total hypernetted-chain structure factor used from the liquid state to the plasma. No interpolation between two limiting structure factors is required. The effect of the suppression of the elastic contributions decreases progressively and naturally as temperature rises.

We obtained satisfactory agreement with experimental conductivities available for solid aluminum. Following Baiko *et al.*'s assumption that long-range order persists in the liquid during the characteristic electron-ion scattering time, an elastic contribution similar to solid state's one must also be removed from the total liquid's structure factor for the calculation of the liquid's resistivity. We derived the correction to the resistivity to be applied in order to account for the existence of such transient long-range order in the liquid. We improved this way considerably the agreement with quantum-molecular dynamics conductivities, especially with those obtained with the same class of exchange-correlation functionals (i.e., LDA) than ours. We observed the same effect on liquid aluminum's isobaric conductivities, which are closer to experiments when this correction is performed. The corrected conductivities are very sensitive to the type of transient long-range order retained. Our results suggest a slight compression of the solid's fcc structure along the vertical c axis rather than perfectly fcc long-range order in liquid aluminum.

Finally, we considered the case of two series of ultrafast experiments performed on aluminum, i.e., Milchberg *et al.*'s ones using short laser pulses, and Sperling *et al.*'s x-ray heating ones carried out on LCLS facility. The former have been the subject of many theoretical works for electron temperatures from 10 to 100 eV, where the resistivity exhibits a maximum. Correct agreement was observed in the present work as well as in previous ones, with the usual one-temperature Ziman formalism. Some authors tried a two-temperature approach in this temperature range, with comparable results. We focus in our work on electron temperatures $T_e \lesssim 10$ eV, where the ion-ion structure factor has more impact on resistivities, and where two-temperature effects are expected to be therefore more important. Assuming that the ion subsystem remains a fcc crystal in these experiments, we used the multiphonon structure factor calculated for the solid state, and obtained, applying two-temperature Ziman's formalism, electrical conductivities in qualitative agreement with Milchberg's experimental values. Such a result implies that the ion subsystem is necessarily different from the solid in LCLS experiments. Our attempts to explain the latter assuming an initial liquid state at some temperature $T_i \ll T_e$ but above melting did no more succeed, suggesting that the actual initial state before main heating is neither a perfect

TABLE II. Number $N(G)$ and length G (in units of $2\pi/a$) of the 10 first reciprocal vectors for the fcc crystal.

$N(G)$	8	6	12	24	8	6	24	24	24	32
G	$\sqrt{3}$	2	$2\sqrt{2}$	$\sqrt{11}$	$2\sqrt{3}$	4	$\sqrt{19}$	$2\sqrt{5}$	$2\sqrt{6}$	$3\sqrt{3}$

solid nor a normal liquid. From their two-temperature neutral pseudo-atom-based calculations, Dharma-wardana *et al.* obtained good agreement with experiments assuming a “supercooled” initial liquid state at T_i below melting. Such a calculation is beyond our reach. In the future, we plan to improve our computation of the HNC structure factor, which might shed new light on the discrepancies between calculations and measurements in the LCLS experiment.

APPENDIX: FIRST LAYERS OF RECIPROCAL VECTORS

1. Case of fcc structure

The elementary fcc cell is defined by the vectors

$$\begin{aligned} \vec{R}_1 &= \frac{a}{2}(0, 1, 1) \\ \vec{R}_2 &= \frac{a}{2}(1, 0, 1) \\ \vec{R}_3 &= \frac{a}{2}(1, 1, 0), \end{aligned} \tag{A1}$$

where a is the lattice parameter, such as $a^3 = 4\Omega_{WS}$, Ω_{WS} denoting the volume of the Wigner-Seitz cell, and the reciprocal cell by the elemental reciprocal vectors,

$$\begin{aligned} \vec{G}_1 &= 2\pi \frac{\vec{R}_2 \times \vec{R}_3}{\vec{R}_1 \cdot (\vec{R}_2 \times \vec{R}_3)} = \frac{2\pi}{a}(-1, 1, 1) \\ \vec{G}_2 &= 2\pi \frac{\vec{R}_3 \times \vec{R}_1}{\vec{R}_1 \cdot (\vec{R}_2 \times \vec{R}_3)} = \frac{2\pi}{a}(1, -1, 1) \\ \vec{G}_3 &= 2\pi \frac{\vec{R}_1 \times \vec{R}_2}{\vec{R}_1 \cdot (\vec{R}_2 \times \vec{R}_3)} = \frac{2\pi}{a}(1, 1, -1). \end{aligned} \tag{A2}$$

TABLE III. Number $N(G)$ and length G (in units of $2\pi/a$) of the 10 first reciprocal vectors for the bcc crystal.

$N(G)$	12	6	24	12	24	8	48	6	36	24
G	$\sqrt{2}$	2	$\sqrt{6}$	$2\sqrt{2}$	$\sqrt{10}$	$2\sqrt{3}$	$\sqrt{14}$	4	$3\sqrt{2}$	$2\sqrt{5}$

The reciprocal vectors \vec{G} are such as

$$\vec{G} = n_1\vec{G}_1 + n_2\vec{G}_2 + n_3\vec{G}_3. \tag{A3}$$

Table II reports the 10 first layers of fcc reciprocal vectors. By “layer” we mean a set of $N(G)$ reciprocal vectors of same length G .

2. Case of bcc structure

The elementary bcc cell is defined by the vectors

$$\begin{aligned} \vec{R}_1 &= \frac{a}{2}(-1, 1, 1) \\ \vec{R}_2 &= \frac{a}{2}(1, -1, 1) \\ \vec{R}_3 &= \frac{a}{2}(1, 1, -1), \end{aligned} \tag{A4}$$

where the lattice parameter a verifies here $a^3 = 2\Omega_{WS}$, and the elemental reciprocal vectors are

$$\begin{aligned} \vec{G}_1 &= 2\pi \frac{\vec{R}_2 \times \vec{R}_3}{\vec{R}_1 \cdot (\vec{R}_2 \times \vec{R}_3)} = \frac{2\pi}{a}(0, 1, 1) \\ \vec{G}_2 &= 2\pi \frac{\vec{R}_3 \times \vec{R}_1}{\vec{R}_1 \cdot (\vec{R}_2 \times \vec{R}_3)} = \frac{2\pi}{a}(1, 0, 1) \\ \vec{G}_3 &= 2\pi \frac{\vec{R}_1 \times \vec{R}_2}{\vec{R}_1 \cdot (\vec{R}_2 \times \vec{R}_3)} = \frac{2\pi}{a}(1, 1, 0). \end{aligned} \tag{A5}$$

The 10 first layers of bcc reciprocal vectors, are given in Table III.

[1] S. H. Glenzer, B. J. MacGowan, P. Michel *et al.*, Symmetric inertial confinement fusion implosions at ultra-high laser energies, *Science* **327**, 1228 (2010).

[2] O. A. Hurricane, D. A. Callahan, D. T. Casey *et al.*, Fuel gain exceeding unity in an inertially confined fusion implosion, *Nature (London)* **506**, 343 (2014).

[3] J. J. Fortney, S. H. Glenzer, M. Koenig, B. Militzer, D. Saumon, and D. Valencia, Frontiers of the physics of dense plasmas and planetary interiors: Experiments, theory, and applications, *Phys. Plasmas* **16**, 041003 (2009).

[4] J. S. Udrea, N. Shilkin, V. E. Fortov, D. H. H. Hoffmann, J. Jacoby, M. I. Kulish, V. Mintsev, P. Ni, D. Nikolaev, N. A. Tahir, and D. Varentsov, Electrical resistivity measurements of heavy ion beam generated high energy aluminum, *J. Phys. A: Math. Gen.* **39**, 4743 (2006).

[5] I. Krisch and H.-J. Kunze, Measurements of electrical conductivity and the mean ionization state of nonideal aluminum plasmas, *Phys. Rev. E* **58**, 6557 (1998).

[6] A. W. DeSilva and J. D. Katsouras, Electrical conductivity of dense copper and aluminum plasmas, *Phys. Rev. E* **57**, 5945 (1998); **59**, 3774 (1999).

[7] V. N. Korobenko, A. D. Rakhel, A. I. Savvatimski, and V. E. Fortov, Measurements of the electrical resistivity of hot aluminum passing from the liquid to gaseous state at supercritical pressure, *Phys. Rev. B* **71**, 014208 (2005); **71**, 099902(E) (2005).

[8] V. N. Korobenko and A. D. Rakhel, Electrical resistivity and equation of state measurements on hot expanded aluminum in the metal-nonmetal transition range, *Phys. Rev. B* **75**, 064208 (2007).

- [9] J. F. Benage, W. R. Shanahan, and M. S. Murillo, Electrical Resistivity Measurements of Hot Dense Aluminum, *Phys. Rev. Lett.* **83**, 2953 (1999).
- [10] P. Renaudin, C. Blancard, G. Faussurier, and P. Noiret, Combined Pressure and Electrical-Resistivity Measurements of Warm Dense Aluminum and Titanium Plasmas, *Phys. Rev. Lett.* **88**, 215001 (2002).
- [11] V. Recoules, P. Renaudin, J. Clerouin, P. Noiret, and G. Zérah, Electrical conductivity of hot expanded aluminum: Experimental measurements and *ab-initio* calculations, *Phys. Rev. E* **66**, 056412 (2002).
- [12] P. Sperling, E. J. Gamboa, H. J. Lee, H. K. Chung, E. Galtier, Y. Omarbakiyeva, H. Reinholz, G. Röpke, U. Zastra, J. Hastings, L. B. Fletcher, and S. H. Glenzer, Free-Electron X-Ray Laser Measurements of Collisional-Damped Plasmons in Isochorically Heated Warm Dense Matter, *Phys. Rev. Lett.* **115**, 115001 (2015).
- [13] H. M. Milchberg, R. R. Freeman, S. C. Davey, and R. M. More, Resistivity of a Simple Metal from Room Temperature to 10^6 K, *Phys. Rev. Lett.* **61**, 2364 (1988).
- [14] P. D. Desai, H. M. James, and C. Y. Ho, Electrical resistivity of aluminum and manganese, *J. Phys. Chem. Ref. Data* **13**, 1131 (1984).
- [15] R. Brandt and G. Neuer, Electrical resistivity and thermal conductivity of pure aluminum and aluminum alloys up to and above the melting temperature, *Int. J. Thermophys.* **28**, 1429 (2007).
- [16] G. R. Gathers, Thermophysical properties of liquid copper and aluminum, *Int. J. Thermophys.* **4**, 209 (1983).
- [17] D. V. Knyazev and P. R. Levashov, *Ab initio* calculation of transport and optical properties of aluminum: Influence of simulation parameters, *Comput. Mater. Sci.* **79**, 817 (2013).
- [18] T. Sjöström and J. Daligault, Ionic and electronic transport properties in dense plasmas by orbital-free density functional theory, *Phys. Rev. E* **92**, 063304 (2015).
- [19] C. E. Starrett, R. Perriot, N. R. Shaffer, T. Nelson, L. A. Collins, and C. Ticknor, Tabular electric conductivity for aluminum, *Contrib. Plasma Phys.* **60**, e201900123 (2020).
- [20] B. B. L. Witte, P. Sperling, M. French, V. Recoules, S. H. Glenzer, and R. Redmer, Observations of non-linear plasmon damping in dense plasmas, *Phys. Plasmas* **25**, 056901 (2018).
- [21] V. Vlcek, N. de Koker, and G. Steinle-Neumann, Electrical and thermal conductivity of Al liquid at high pressures and temperatures from *ab initio* computations, *Phys. Rev. B* **85**, 184201 (2012).
- [22] R. Redmer, Electrical conductivity of dense metal plasmas, *Phys. Rev. E* **59**, 1073 (1999).
- [23] S. Kuhlbrodt and R. Redmer, Transport coefficients for dense metal plasmas, *Phys. Rev. E* **62**, 7191 (2000).
- [24] E. M. Apfelbaum, Calculation of electronic transport coefficients of Ag and Au plasmas, *Phys. Rev. E* **84**, 066403 (2011).
- [25] D. N. Zubarev, *Nonequilibrium Statistical Thermodynamics* (Plenum, New-York, 1974).
- [26] G. A. Rinker, Electrical conductivity of a strongly coupled plasma, *Phys. Rev. B* **31**, 4207 (1985).
- [27] G. A. Rinker, Systematic calculation of plasma transport coefficients for the Periodic Table, *Phys. Rev. A* **37**, 1284 (1988).
- [28] P. A. Sterne, S. B. Hansen, B. G. Wilson, and W. A. Isaacs, Equation of state, occupation probabilities and conductivities in the average atom Purgatorio code, *High Energy Dens. Phys.* **3**, 278 (2007).
- [29] P. L. Bhatnagar, E. P. Gross, and M. Krook, A model for collision processes in gases. I. Small amplitude processes in charged and neutral one-component systems, *Phys. Rev.* **94**, 511 (1954).
- [30] J. M. Ziman, A theory of the electrical properties of liquid metals. I: The monovalent metals, *Philos. Mag.* **6**, 1013 (1961).
- [31] R. Evans, B. L. Gyroffly, N. Szabo, and J. M. Ziman, On the resistivity of liquid transition metals, in *The Properties of Liquid Metals*, edited by T. Takeuchi (Wiley, New York, 1973), pp. 319–331.
- [32] R. Kubo, Statistical-mechanical theory of irreversible processes. I. General theory and simple applications to magnetic and conduction problems, *J. Phys. Soc. Jpn.* **12**, 570 (1974).
- [33] D. A. Greenwood, The Boltzmann equation in the theory of electrical conduction in metals, *Proc. Phys. Soc. Lond.* **71**, 585 (1958).
- [34] C. E. Starrett, J. Clerouin, V. Recoules, J. D. Kress, L. A. Collins, and D. E. Hanson, Average atom transport properties for pure and mixed species in the hot and warm dense regimes, *Phys. Plasmas* **19**, 102709 (2012).
- [35] D. J. Burill, D. V. Feinblum, M. R. J. Charest, and C. E. Starrett, Comparison of electron transport calculations in warm dense matter using the Ziman formula, *High Energy Dens. Phys.* **19**, 1 (2016).
- [36] J.-C. Pain and G. Dejonghe, Electrical resistivity in warm dense plasmas beyond the average-atom model, *Contrib. Plasma Phys.* **50**, 39 (2010).
- [37] F. Perrot and M. W. C. Dharma-wardana, Theoretical issues in the calculation of the electrical resistivity of plasmas, *Int. J. Thermophys.* **20**, 1299 (1999).
- [38] G. Faussurier and C. Blancard, Electrical resistivity calculations in dense plasmas, *Phys. Rev. E* **100**, 033202 (2019).
- [39] M. W. C. Dharma-wardana, D. D. Klug, L. Harbour, and L. J. Lewis, Isochoric, isobaric and ultrafast conductivities of aluminum, lithium and carbon in the warm dense matter regime, *Phys. Rev. E* **96**, 053206 (2017).
- [40] C. E. Starrett and D. Saumon, Fully variational average atom model with ion-ion correlation, *Phys. Rev. E* **85**, 026403 (2012).
- [41] A. M. Rosenfeld and M. J. Stott, Change in resistivity of simple metals on melting, *Phys. Rev. B* **42**, 3406 (1990).
- [42] D. A. Baiko, A. D. Kaminker, A. Y. Potekhin, and D. G. Yakovlev, Ion Structure Factors and Electron Transport in Dense Coulomb Plasmas, *Phys. Rev. Lett.* **81**, 5556 (1998).
- [43] A. Y. Potekhin, D. A. Baiko, P. Haensel, and D. G. Yakovlev, Transport properties of degenerate electrons in neutron star envelopes and white dwarf cores, *Astron. Astrophys.* **346**, 345 (1999).
- [44] A. A. Ovechkin, P. A. Loboda, and A. L. Falkov, Transport and dielectric properties of dense ionized matter from the average-atom RESEOS model, *High Energy Dens. Phys.* **20**, 38 (2016).
- [45] D. A. Liberman, Self-consistent field model for condensed matter, *Phys. Rev. B* **20**, 4981 (1979).
- [46] R. Piron and T. Blenski, Variational Average Atom In Quantum Plasmas (VAAQP) code and virial theorem: Equation-of-state and shock-Hugoniot calculations for warm dense Al, Fe, Cu and Pb, *Phys. Rev. E* **83**, 026403 (2011).

- [47] S. B. Hansen, W. A. Isaacs, P. A. Sterne, B. G. Wilson, V. Sonnad, and D. A. Young, Electrical conductivity calculations from the Purgatorio code, in *Proceedings of the NEPDC 2005* (Lawrence Livermore National Laboratory, Livermore, 2006).
- [48] M. Pénicaud, An average-atom code for warm matter: Application to aluminum and uranium, *J. Phys.: Condens. Matter* **21**, 095409 (2009).
- [49] J.-C. Pain, Quantum-statistical equation-of-state models of dense plasmas: High-pressure Hugoniot shock adiabats, *Contrib. Plasma Phys.* **47**, 421 (2007).
- [50] N. Wetta and J.-C. Pain, Thermal electronic properties of aluminum under pressure: The role of sp to $3d$ electron transfer, *Phys. Rev. B* **100**, 205127 (2019).
- [51] R. M. More, Pressure ionization, resonances and the continuity of bound and free states, *Adv. At. Mol. Phys.* **21**, 305 (1985).
- [52] G. Baym, Direct calculation of electronic properties of metals from neutron scattering data, *Phys. Rev.* **135**, A1691 (1964).
- [53] R. C. Shukla, Analysis of the Debye-Waller factor and multiphonon-series contributions in the phonon-limited resistivity of metals, *Phys. Rev. B* **22**, 5810 (1980).
- [54] C. Kittel, *Quantum Theory of Solids* (Wiley, New-York, 1963), Vol. 5.
- [55] Ph. Mangin, C. Tête, and G. Marchal, Elastic and inelastic contributions to the structure factor of amorphous materials, *Solid State Commun.* **50**, 1073 (1984).
- [56] N. E. Phillips, Heat capacity of aluminum between 0.1 K and 0.4 K, *Phys. Rev.* **114**, 676 (1959).
- [57] I. Gonzalez, I. Kondrashuk, V. H. Moll, and A. Vega, Analytic expressions for Debye functions and to the heat capacity of a solid, [arXiv:1908.08667](https://arxiv.org/abs/1908.08667).
- [58] L. V. Meisel and P. J. Cote, Structure factors in amorphous and disordered harmonic Debye solids, *Phys. Rev. B* **16**, 2978 (1977).
- [59] L. V. Meisel and P. J. Cote, Critical test of the diffraction model in amorphous and disordered metals, *Phys. Rev. B* **17**, 4652 (1978).
- [60] S. R. Nagel, Temperature dependence of the resistivity in metallic glasses, *Phys. Rev. B* **16**, 1694 (1977).
- [61] P. Schmidt, G. Zwicknagel, P.-G. Reinhard, and C. Toepffer, Longitudinal and transversal collective modes in strongly correlated plasmas, *Phys. Rev. E* **56**, 7310 (1997).
- [62] F. J. Rogers, A HNC study of asymmetrical charged hard spheres, *J. Chem. Phys.* **73**, 6272 (1980).
- [63] B. Held and P. Pignolet, Semi-empirical correlation function for one and two-ionic component plasma, *J. Phys.* **47**, 437 (1986).
- [64] D. A. Baiko and D. G. Yakovlev, Thermal and electric conductivities of Coulomb crystals in neutron stars and white dwarfs, *Astron. Lett.* **21**, 702 (1995).
- [65] E. L. Pollock and J. P. Hansen, Statistical mechanics of dense ionized matter. II. Equilibrium properties and melting transition of the crystallized one-component plasma, *Phys. Rev. A* **8**, 3110 (1973).
- [66] M. Leitner, T. Leitner, A. Schmon, K. Aziz, and G. Pottlacher, Thermophysical properties of liquid aluminum, *Metall. Mater. Trans. A* **48**, 3036 (2017).
- [67] P. Sperling, S. Rosmej, R. Bredow, L. B. Fletcher, E. Galtier, E. J. Gamboa, H. J. Lee, H. Reinholz, G. Röpke, U. Zastra, and S. H. Glenzer, Electrical conductivity calculations in isochorically heated warm dense aluminum, *J. Phys. B: At. Mol. Opt. Phys.* **50**, 134002 (2017).
- [68] N. R. Shaffer and C. E. Starrett, Model of electron transport in dense plasmas spanning temperature regimes, *Phys. Rev. E* **101**, 053204 (2020).
- [69] J. P. Perdew, K. Burke, and M. Ernzerhof, Generalized Gradient Approximation Made Simple, *Phys. Rev. Lett.* **77**, 3865 (1996); **78**, 1396 (1997).
- [70] J. Heyd, G. E. Scuseria, and M. Ernzerhof, Hybrid functionals based on a screened Coulomb potential, *J. Chem. Phys.* **118**, 8207 (2003).
- [71] J. P. Perdew and A. Zunger, Self-interaction correction to density-functional approximations for many-electron systems, *Phys. Rev. B* **23**, 5048 (1981).
- [72] V. V. Karasiev, T. Sjostrom, J. Dufty, and S. B. Trickey, Accurate Homogeneous Electron Gas Exchange-Correlation Free Energy for Local Spin-Density Calculations, *Phys. Rev. Lett.* **112**, 076403 (2014).
- [73] J.-L. Bretonnet and A. Derouiche, Analytic form for the one-component plasma structure factor, *Phys. Rev. B* **38**, 9255 (1988).
- [74] F. Lado, S. M. Foiles, and N. W. Ashcroft, Solutions of the reference-hypernetted-chain equation with minimized free energy, *Phys. Rev. A* **28**, 2374 (1983).
- [75] G. Faussurier and C. Blancard, Resistivity saturation in warm dense matter, *Phys. Rev. E* **91**, 013105 (2015).
- [76] M. W. C. Dharma-wardana and F. Perrot, Resistivity and dynamic conductivity of laser-pulse heated aluminum up to 10^6 and along the shock Hugoniot up to 20 Mbars, *Phys. Lett. A* **163**, 223 (1992).
- [77] M. W. C. Dharma-wardana, Dynamic conductivity and plasmon profile of aluminum in the ultra-fast-matter regime, *Phys. Rev. E* **93**, 063205 (2016).
- [78] Y. V. Petrov, N. A. Inogamov, A. V. Mokshin, and B. N. Galimzyanov, Electrical resistivity and thermal conductivity of liquid aluminum in the two-temperature state, *J. Phys.: Conf. Ser.* **946**, 012096 (2018).
- [79] D. V. Knyazev and P. R. Levashov, Transport and optical properties of warm dense aluminum in the two temperature regime: *Ab initio* calculation and semiempirical approximation, *Phys. Plasmas* **21**, 073302 (2014).